

Structure-Based Design and Synthesis of Novel Dual-Target Inhibitors against Cyanobacterial Fructose-1,6-Bisphosphate Aldolase and Fructose-1,6-Bisphosphatase

Ding Li,^{†,‡,§} Xinya Han,^{†,§} Qidong Tu,^{†,||,§} Lingling Feng,[†] Di Wu,[†] Yao Sun,[†] Haifeng Chen,[†] Yongjian Li,[†] Yanliang Ren,^{*,†} and Jian Wan^{*,†}

[†]Key Laboratory of Pesticide & Chemical Biology (CCNU), Ministry of Education, College of Chemistry, Central China Normal University, Wuhan 430079, China

[‡]Department of Chemistry and Chemical Engineering, College of Science, Northwest A&F University, 3 Taicheng Road, Yangling 712100, Shanxi, China

^{||}School of Pharmacy, Jiangxi Science and Technology Normal University, Nanchang, Jiangxi 330013, China

Supporting Information

ABSTRACT: Cyanobacteria class II fructose-1,6-bisphosphate aldolase (Cy-FBA-II) and cyanobacteria fructose-1,6-bisphosphatase (Cy-FBPase) are two neighboring key regulatory enzymes in the Calvin cycle of the cyanobacteria photosynthesis system. Each of them might be taken as a potential target for designing novel inhibitors to chemically control harmful algal blooms (HABs). In the present paper, a series of novel inhibitors were rationally designed, synthesized, and optimized based upon the structural and interactional information of both Cy-FBA-II and Cy-FBPase, and their inhibitory activities were examined in vitro and in vivo. The experimental results showed that compounds L19e–L19g exhibited moderate inhibitory activities ($IC_{50} = 28.1\text{--}103.2 \mu\text{M}$) against both Cy-FBA-II and Cy-FBPase; compounds L19a–L19d, L19h, L20a–L20d exhibited high Cy-FBA-II inhibitory activities ($IC_{50} = 2.3\text{--}16.9 \mu\text{M}$) and moderate Cy-FBPase inhibitory activities ($IC_{50} = 31.5\text{--}141.2 \mu\text{M}$); however, compounds L20e–L20h could potently inhibit both Cy-FBA-II and Cy-FBPase with IC_{50} values less than $30 \mu\text{M}$, which demonstrated more or less dual-target inhibitor's feature. Moreover, most of them exhibited potent algicide activity ($EC_{50} = 0.8\text{--}22.3 \text{ ppm}$) against cyanobacteria *Synechocystis* sp. PCC 6803.

KEYWORDS: fructose-1,6-bisphosphate aldolase, fructose-1,6-bisphosphatase, structure-based design, dual-target inhibitors, algicides

INTRODUCTION

Cyanobacteria harmful algal blooms (HABs) pose an increasingly serious water pollution problem all over the world.^{1,2} Approaches to control these HABs fall into three categories: mechanical, physical/chemical, and biological controls. Recently, chemical control was regarded as one of the most effective methods. Chemical control involves the use of compounds, such as copper compounds, chemical oxidants, and herbicides.¹ However, none of these compounds are specifically designed or developed for exclusive targeting of enzymes of cyanobacteria; thus the utility of chemical control has significant limits. In the chemical biology approach, however, specific target (critical enzymes) of cyanobacteria may provide useful solutions to the development of potential algicides.

In photoautotrophic organisms, fructose-1,6-bisphosphate aldolase (FBA, EC 4.1.2.13) and fructose-1,6-bisphosphatase (FBPase, EC 3.1.3.11) are two essential regulatory enzymes in the Calvin cycle, as illustrated in Figure 1. FBA occurs in two distinct classes in the biosphere and catalyzes the reversible aldol condensation of dihydroxyacetone phosphate (DHAP) and glyceraldehyde 3-phosphate (GAP) to fructose-1,6-biphosphate (FBP).^{2,3} Class I FBA (FBA-I), which are present in higher organisms (plants and animals) and some prokaryotes, form a Schiff base intermediate between the keto

substrate (FBP or DHAP) and a lysine residue in the active site, while class II FBA (FBA-II) requires a divalent metal ion (usually zinc or cobalt ion) to polarize the keto carbonyl group of the substrate (FBP or DHAP) and to stabilize the enediolate intermediate formed during catalysis. Because of their occurrence in many pathogenic microbes (bacteria, yeasts, parasites) and their absence in animals, FBA-II has been regarded as a particularly attractive new target, and a lot of attention was focused on the drug design of the enzyme.^{4,5} On the other hand, FBPase, the other potential enzyme in the Calvin cycle, catalyzes the reversible hydrolysis of FBP into fructose 6-phosphate and inorganic phosphate.^{6,7}

In cyanobacteria photoautotrophic organisms, the whole genome sequence database has revealed the presence of putative genes encoding of FBA-I and FBA-II.^{8,9} It seems, however, that FBA-II generally exist in cyanobacteria and represent the major or complete part of total extractable FBA activity.^{6,9} Also, Nakahara et al.⁹ reported that FBA-I was functionally redundant in *Synechocystis* sp. PCC 6803, while attempts to disrupt the FBA-II gene had not been successful.

Received: May 3, 2013

Revised: July 3, 2013

Accepted: July 4, 2013

Published: July 4, 2013

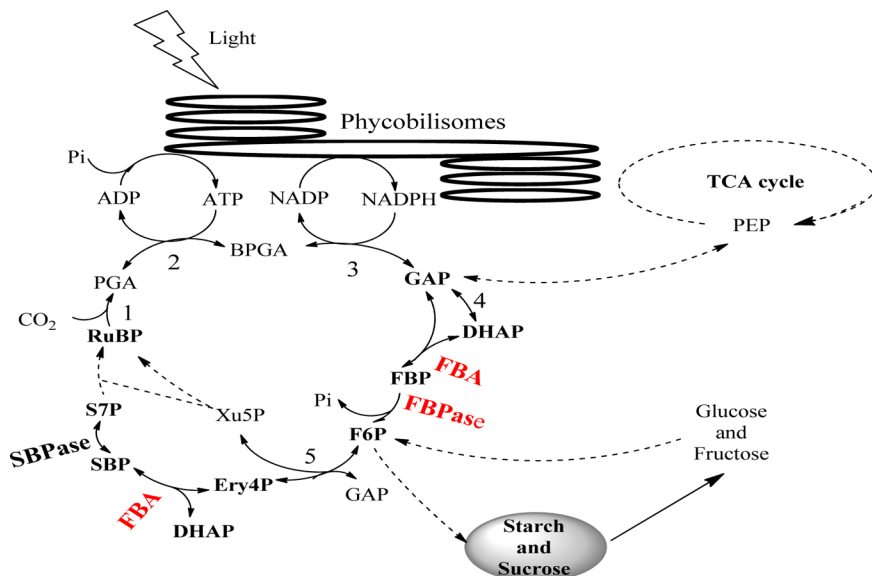


Figure 1. Simplified model of Calvin cycle in cyanobacteria. The reactions were catalyzed by enzymes numbered as follows: (1) Rubisco (ribulose-1,5-bisphosphate carboxylase/oxygenase). (2) PGA kinase (3-phosphoglycerate kinase). (3) NADP-G3P dehydrogenase (NADP-glyceraldehyde-3-phosphate dehydrogenase). (4) TPI (triose-phosphate isomerase). 5) TKT (transketolase).

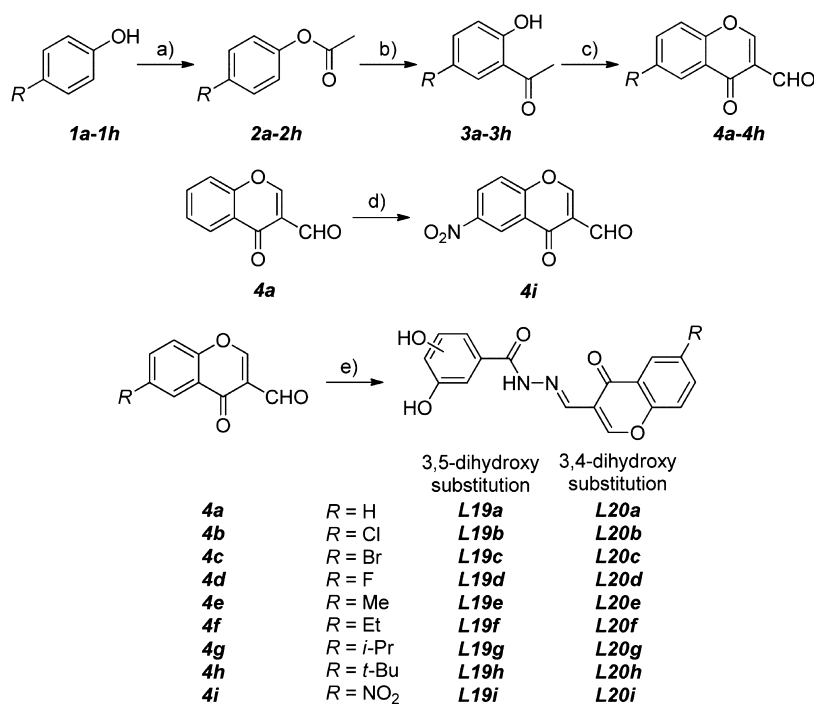


Figure 2. Synthetic route for the title compounds L19a—L19i and L20a—L20i. (a) Ac_2O , concentrated H_2SO_4 . (b) Anhydrous AlCl_3 , 120 °C. (c) POCl_3 , DMF. (d) Fuming HNO_3 , concentrated H_2SO_4 , 0 °C. (e) 3,5-(or 3,4-)dihydroxybenzohydrazide, EtOH , AcOH .

On the other hand, previous studies^{6,10} have demonstrated that the disruption of FBPase gene is lethal to both *Synechocystis* sp. PCC 6803 and *Synechococcus* PCC 7942. Expression of FBPase from cyanobacteria (Cy-FBPase) in transgenic tobacco significantly enhances photosynthetic efficiency and grows under atmospheric conditions.¹¹ In view of these crucial roles and functions of Cy-FBPase and FBA-II from cyanobacteria (Cy-FBA-II), each of them might be taken as a potential target for designing novel inhibitors to chemically control harmful HABs. Recently, dual or multitarget inhibitors^{12,13} have gained increased attention due to their lower resistance. Since Cy-

FBA-II and Cy-FBPase were neighboring key regulatory enzymes with the same substrate FBP in the pathway of the Calvin cycle, these two enzymes are most likely to be taken as appropriate dual targets for rationally designing novel dual-target inhibitors. Here, with a systematically structure-centric approach, a specific protocol of molecular docking-based dual-target virtual screening was generated and performed for both target enzymes. A series of potential hit compounds interacting with both enzymes were virtually filtered out from the Specs database, and their inhibitory activities were examined *in vitro* and *in vivo*. Followed by a further study of combining

structure–activity relationship (SAR) analysis and optimized synthesis, we identified the first set of novel dual-target inhibitors targeting on both Cy-FBA-II and Cy-FBPase.

MATERIALS AND METHODS

Amino Acid Sequence Alignment and Homology Modeling.

The amino acid sequence of Cy-FBA-II, retrieved from the NCBI database (accession number NP_442114) was aligned with that of Gl-FBA-II (accession number XP_001710050) by using ClustalW2 program.¹⁴ Based on the sequence alignment, a three dimensional (3D) structure of Cy-FBA-II was built using SWISSMODEL server.^{15,16} The dimeric model of Cy-FBA-II catalytic subunits was constructed through combination of two chains. The cofactors, Zn²⁺, were derived from the template crystal structure, and then replaced by Co²⁺. Two chains of dimeric protein were then staged optimized with SYBYL 7.3 using AMBER force field.^{17,18} The modeling 3D structure of Cy-FBA-II was further validated by Procheck,¹⁹ ProSA,²⁰ ProQ,²¹ and Qmean program.²²

Docking-Based Virtual Screening. To generate the region of active site and the corresponding virtual screening cavity of the donor pharmacophore model, the resultant homology modeling structure of Cy-FBA-II and X-ray crystallographic structure of template Gl-FBA-II (PDB ID: 3GAY) were superposed on each other, and then the tagatose-1,6-bisphosphate (TBP), a known substrate analogue inhibitor, was merged into the corresponding site of Cy-FBA-II. The crystal complex of Cy-FBPase and substrate FBP was taken from the Brookhaven Protein Database (PDB ID: 3RPL). Then, all atoms located within the range of 6.5 Å from any atom of TBP or substrate FBP were selected into the active site of both Cy-FBA-II and Cy-FBPase, and corresponding amino acid residues were, therefore, involved into the active site if only one of their atoms was selected.

FlexX embodied in SYBYL 7.3 package is a fast and automated docking method, which takes the ligand's conformational flexibility into account during the docking process by an incremental fragment placing technique.²³ FlexX-Pharm²⁴ enables pharmacophore-type constraints to be used in FlexX to quickly guide ligand docking. Thus, FlexX-Pharm was first used to define spatial and pharmacophore constraint in the docking-based virtual screening process of Cy-FBA-II. Surflex-Dock²⁵ uses an empirical scoring function and a patented search engine to dock ligands into a protein's binding site. It is particularly successful at eliminating false positive results and can, therefore, be used to narrow down the screening pool, while still retaining a large number of active compounds. Thus, after FlexX-Pharm processes, a set of nonconstraints molecular docking processes, Surflex-Dock, were subsequently performed in the same cavity of Cy-FBA-II to re-evaluate accurately receptor–ligand binding interactions. The virtual screening strategy adopted in the present study also principally consisted of one step of two-dimensional (2D) ligand-based searching in terms of Lipinski rules. A similar strategy has also been used in our previous studies.^{26,27} All calculations were performed on a CCNUGrid-based computational environment (CCNUGrid Web site <http://202.114.32.71:8090/ccnu/chem/platform.xml>).

Chemistry. For a detailed description of chemicals and analytical equipment used, see the Supporting Information. This section reports the synthesis of L20b (Figure 2). All other synthetic compounds and analytical data are included in the Supporting Information. 4a was prepared according to a three-step reaction using substituted phenol as starting materials, which is similar to the synthesis method of 3-formylchromone.²⁸ The 3,5-(and 3,4)-dihydroxybenzohydrazide were purchased from Alfa Aesar Company.

N'-(6-Chloro-4-oxo-4H-chromen-3-yl)methylene)-3,4-dihydroxybenzohydrazide (L20b). To 4b (208 mg, 1 mM) and 3,4-dihydroxybenzohydrazide (168 mg, 1 mM) in ethanol (25 mL) was added three drops of acetic acid with stirring for 6 h at room temperature. Insoluble solid was gradually generated, then filtered, and washed several times with ethanol. After drying, white powder L20b was obtained (329 mg, yield 92%). Mp: 214–217 °C. ¹H NMR (600 MHz, DMSO-*d*₆): δ = 11.74 (s, 1H, NH), 9.68 (s, 1H, OH), 9.27 (s, 1H, OH), 8.85 – 6.73 (m, 8H, =CH-O, CH=N, ArH). HRMS

(MALDI): *m/z* = 381.0257, calcd for C₁₇H₁₁ClN₂O₅ [M + Na]⁺ 381.0254.

Enzyme Inhibition Activity. To evaluate the inhibitory activity of hit compounds screened and synthesized in the present study, the half maximal inhibitory concentration (IC₅₀) values of hit compounds were determined at Cy-FBA-II and Cy-FBPase recombinant protein level. Cy-FBA-II and Cy-FBPase were expressed in *Escherichia coli* BL21(DE3) cells as described previously.^{9,29} Glycerol 3-phosphate dehydrogenase (GPDH) and triosephosphate isomerase (TIM) were commercial preparations, available from Sigma. The activity of the cleavage reaction of Cy-FBA-II was assayed in the mixture 50 mM Tris-HCl buffer (pH 7.5), 0.2 mM CoCl₂, 0.2 mM NADH, 0.5 unit each of GPDH and TIM, and 0.4 mM FBP in a final volume of 0.22 mL. The activity of the cleavage reaction was measured by monitoring the decrease in absorbance of NADH at 340 nm on the microplate reader (Bioteck Synergy2, USA) over 5 min.

The enzyme activities of Cy-FBPase were measured by a colorimetric assay based on the detection of inorganic phosphate hydrolyzed from FBP by the enzyme.^{30–32} The phosphate released was quantified spectrophotometrically as a complex with ammonium molybdate and malachite green. To calculate the μM of product formation, calibration curves were made with a standard KH₂PO₄ solution in the range of 2–60 μM. The absorbance at 620 nm of the reaction mixture was measured using a microplate reader.

To determine the corresponding inhibitor constants (IC₅₀), initial rate data taken at saturating substrate, fixed effector, and systematically varied inhibitor concentrations were fit to a Hill equation: $V = V_0 - (V_0 - V_\infty)/[(IC_{50}/I)^n + 1]$,³³ where V , V_0 , and V_∞ are the velocity, maximum velocity (at $I = 0$), and limiting velocity (at I saturating); n is the Hill coefficient associated with the inhibitor; and IC₅₀ is the inhibitor concentration at 50% inhibition. All kinetic data were fit to the growth/sigmoidal model from Origin 7.0 software.

Inhibitory Assays on *Synechocystis* sp. PCC 6803. *Synechocystis* sp. PCC 6803 obtained from Dr. Haibo Jiang were cultured photoautotrophically in BG11 medium³⁴ at 28 °C in 96-well microtiter plates. The inhibitory effect of hit compounds on the cyanobacteria growth was estimated by inhibition over control, which is defined by the following equation: inhibition (%) over control = [1 – (OD₆₈₀ⁱ/OD₆₈₀^c) × 100, where OD₆₈₀ⁱ and OD₆₈₀^c are optical density at 680 nm (OD₆₈₀) values of the cyanobacteria in the control and hit compound treated cultures, respectively, which were measured using the microplate reader. When cyanobacteria growth was significantly inhibited, the effective concentration causing a 50% inhibitory response at 7 days (EC₅₀, 7 days) was estimated with logistic fitting.

RESULTS AND DISCUSSION

Homology Modeling of 3D-Conformation of Cy-FBA-II. A recent review³⁵ has suggested that sequence identity higher than 30% between two proteins was indicative of similar 3D structures. The ClustalW2 analysis showed that class II fructose-1,6-biphosphate aldolase from *Giardia lamblia* (Gl-FBA-II) shared highest identity (46%) with Cy-FBA-II, which allows for a rather straightforward sequence alignment and guarantees the quality of homology modeling. The sequence alignment displayed that the substrate binding sites of Cy-FBA-II and Gl-FBA-II were highly conserved (Figure S1 in the Supporting Information). Therefore, selecting the crystal structure of Gl-FBA-II (complex with a competitive inhibitor, PDB: 3GAY) as template, a plausible homology model of Cy-FBA-II was generated by using SWISSMODEL server.

In order to reduce steric clashes and further obtain a rational modeling 3D conformation of Cy-FBA-II, the staged minimizations have been further performed by using SYBYL 7.3. The metal cofactors of Cy-FBA-II were found to coordinate with H84, H198, and H22 (H84, H178, and H210 in the template protein), respectively, thus all heavy atoms of these three amino acids of Cy-FBA-II were restricted during the

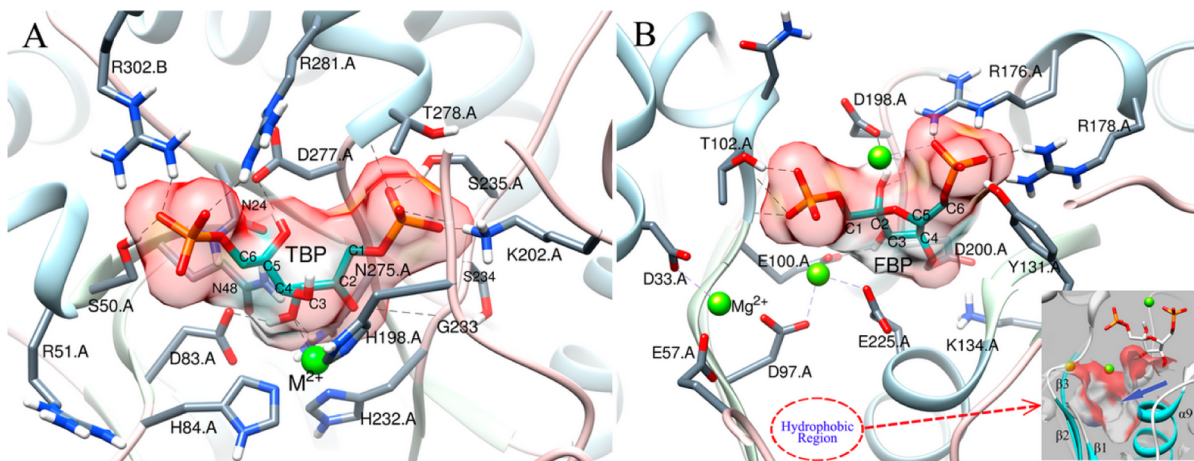


Figure 3. Optimal binding models of TBP into the active site of Cy-FBA-II docked by Surflex module (A) and FBP into the Cy-FBPase in crystallographic structure (B). The light sky blue ribbons represent the helix and sheet of protein, and pink represents the coil of protein. The dashed lines represent the important hydrogen bonds of the ligands and corresponding enzyme. Inset: Surface of the small hydrophobic cavity between three β -strands (β_1 – β_3) and one α -helix (α_9), which is labeled by blue arrow in the vicinity of the hydrophilic active site.

minimization processes to ensure the stereoconfiguration of coordination bonds. Furthermore, the quality of homology modeling Cy-FBA-II was assessed by Procheck, ProQ, ProSA-web, and QMEAN. The assessment results showed that LGscore in ProQ was 5.198 (≥ 2.5 for very good model), QMEAN score was 0.769 (estimated model reliability lies between 0 and 1), and Z-score in ProsaWeb was -8.72 (Figure S2 in the Supporting Information), which suggests that the model of Cy-FBA-II is good enough for further studies. The Ramachandran plot analyses by Procheck (Figure S3 in the Supporting Information) also confirmed the quality of the modeling 3D structure of Cy-FBA-II, and the results showed that 90.7% of residues were distributed in the most favored regions, 7.8% in the additional allowed regions, 0.8% in the generously allowed regions, and only 0.8% in the disallowed regions, respectively. These results demonstrate that the 3D structure of Cy-FBA-II is available for subsequent docking and virtual screening investigations.

Identifying the Binding Models of Cy-FBA-II and TBP.

To validate our docking protocol, a rigorous Surflex docking study for the acyclic keto form of TBP, a known competitive inhibitor of Gl-FBA-II, was carried out. The initial geometric parameters of TBP backbone were extracted out of crystal template protein, on which the hydrogen atoms were added, and subsequently submitted to a minimization by using Tripos force field.³⁶ Our docking results revealed that the binding modes of TBP into the active site of Cy-FBA-II obtained by Surflex-Dock (Figure 3A) were almost identical to the crystallographic results (PDB ID: 3GAY), which gave us confidence in our protocol.

As can be seen from Figure 3A, two ends of TBP were pinned into place via interactions of C1 and C6 phosphate groups, in which C1 phosphate looks likely to form three hydrogen bonds with surrounding residues K202, S235, and T278, while C6 phosphate might form several hydrogen bonds with surrounding residues S50, R281, and R302. Moreover, the conformation of TBP at the catalytic center [viz., the area constituted by conversed residues: D83, H84, H198, and H232] was further defined through two hydrogen bonds of C2=O···NH(G233) and C5–OH···COO(D277), respectively. The C2=O of TBP not only formed a hydrogen bond with backbone amide group of residue G233 but also coordinated

with Co²⁺. Additionally, the C3–OH group was anchored by its interaction with residues D83, N275, and Co²⁺. To further identify the importance of the converged residues surrounding TBP, we mutated the residues S50, D83, K202, G233, S235, N275, D277, T278, R281, and R302 to Ala. The site-directed mutagenesis experiments (Figure S4 in the Supporting Information) showed that mutant D83A, K202A, S235A, and T278A had almost no detectable or weak activities; especially the T278A variant exhibited the lowest activity. The experimental and docking results further suggested that the metal (Co²⁺) and conversed residues D83, K202, S235, and T278 were essential to the catalytic reactions of Cy-FBA-II. It is noteworthy that, apart from the residue D83, the residues K202, S235 and T278 were involved in the interactions with C1-phosphate. Previous study about FBA-II from *Giardia lamblia*⁵ has indicated that the metal ion (Co²⁺) position and C1-phosphate position were critical for the inhibitor binding. Since the residues K202, S235, and T278 were located into the C1-phosphate region, we believe that Co²⁺ and residues K202, S235, and T278 should be necessary for the inhibitor binding, and they could be regarded as the important pharmacophore for the design of Cy-FBA-II inhibitors.

Identifying the Binding Models of Cy-FBPase and Substrate FBP.

In previous studies, we have crystallized and determined the first crystal complex of Cy-FBPase and substrate FBP (PDB ID: 3RPL), in which the substrate FBP with the cyclic hemiketol form bound into the active site of Cy-FBPase. The remarkable hydrogen bonds of FBP and surrounding residues (R176, R178, Y131, T102, and D200) might be observed, as illustrated in Figure 3B. One can notice from Figure 3B that three important magnesium ions existed in the substrate active site of Cy-FBPase. The top one could coordinate with not only residue D198 but also the 6-phosphoryl oxygen of FBP. From this picture we can conclude that this magnesium ion might function in stabilization of substrate FBP. However, it is difficult that this magnesium ion was fixed in the present position when the substrate FBP was replaced by inhibitor, which in turn implied that the residue D198 was a critical residue for the stabilization of FBP. An additional two magnesium ions were bound to the side chains of negatively charged residues, such as D33, E57, D97, E100, and E255. In conclusion, two magnesiums in the bottom of the

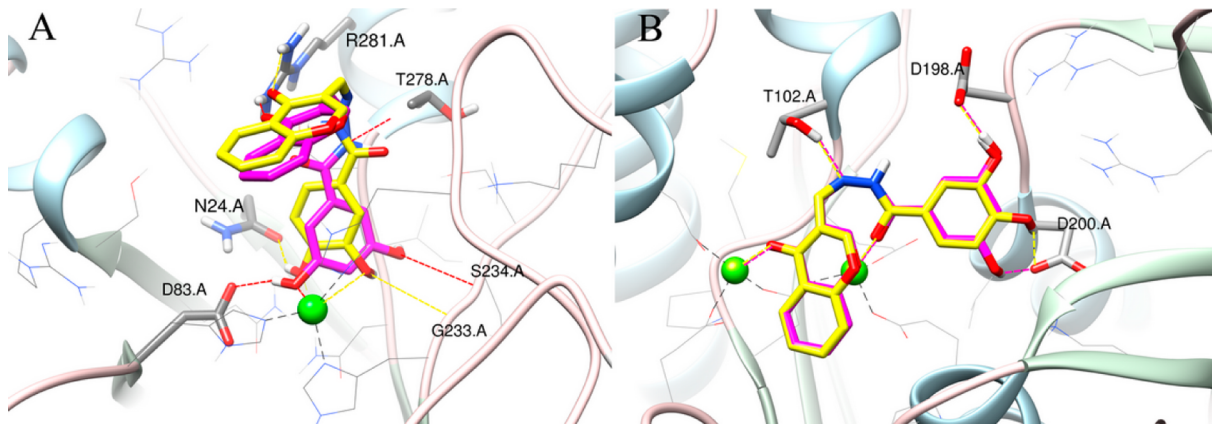


Figure 4. The probable binding modes of compounds L19a and L20a target into the active site of Cy-FBA-II (A) and Cy-FBPase (B). The magenta sticks represent compound L19a, and the yellow sticks represent compound L20a; the dashed lines indicate the important hydrogen bonds between ligand and target enzyme.

active site and the residues R176, R178, Y131, T102, D200, and D198 are likely crucial for the Cy-FBPase inhibitor design. Additionally, in the vicinity of the hydrophilic active site, there was a small hydrophobic cavity between three β -strands (β_1 – β_3) and one α -helix (α 9), as shown in Figure 3B (inset).

Structure-Based Virtual Screening of Dual-Target Inhibitors against Both Cy-FBA-II and Cy-FBPase. The previous interaction analysis of Cy-FBA-II/Cy-FBPase and substrate/inhibitor provides the needed insight into the steric and electrostatic features of the active sites that govern ligand binding. Based upon the structural and interactional information of both Cy-FBA-II and Cy-FBPase and their corresponding substrate or inhibitor, a specific protocol of dual-target virtual screen (as illustrated in Figure S5 in the Supporting Information) was generated and performed to obtain dual-target hit compounds bound into both enzymes. In the first step of virtual screening strategy, the 2D ligand-based searching in terms of Lipinski rules³⁷ was performed to preselect the compounds out of the Specs database. After the 2D ligand-based searching, about 111,000 compounds were obtained for the following docking-based virtual screening. Subsequently, all preselected 2D compounds were transformed to 3D conformation by the CONCORD module of SYBYL 7.3. The proper virtual screening cavities were generated in terms of the active site of 3D modeling structure of Cy-FBA-II and the crystal conformation of Cy-FBPase. Since the substrate pocket of Cy-FBA-II is smaller and has only one metal (Co^{2+}) compared with that of Cy-FBPase, the hit compounds were screened first on basis of the active site of Cy-FBA-II. FlexX-Pharm³⁸ was a very popular pharmacophore-based constraints docking method, which has been regarded as an effective way of rapidly filtering out many unwanted structures in a large database. To raise the efficiency of virtual screening, FlexX-Pharm docking was adopted first to filter the Cy-FBA-II inhibitors out of the Specs database. As discussed above, the metal (Co^{2+}) and residues K202, S235, and T278 were regarded as the important pharmacophore for the design of Cy-FBA-II inhibitors, especially for T278. Thus, current important FlexX-Pharm constraint consisted of a spatial constraint defined by the distance to Co^{2+} within 3.0 Å and an interaction constraint defined by H donor of the T278 side chain, which were set as essential while other important residues were set as optional pharmacophore constraints. Accepted poses fulfilled at least one of these two essential constraints in the cavity of Cy-

FBA-II. After FlexX-Pharm processes for Cy-FBA-II (about 30,000 compounds were selected out), the Surflex-Dock for Cy-FBA-II was further performed, since Surflex-Dock could give significant improvements of the binding affinity of poses to target and successfully eliminate false positive results while still retaining a large number of active compounds.^{25,39} After the Surflex-Dock processes, the top 10,000 compounds were primitively selected out. In order to obtain the hit compounds bound simultaneously into Cy-FBA-II and Cy-FBPase, the Surflex-Dock for Cy-FBPase was subsequently performed for those hit compounds screened for Cy-FBA-II. In the preceding virtual screening, the top 500 compounds were selected out for further comparison analysis. Those compounds with similar backbone were collected into one category, and the “best” hit compounds (~500) were selected out among them by jointly considering dock scoring and docked conformation. According to the interactions discussed above, the C6-phosphate region is essential for the Cy-FBPase. Thus, only if the compound had higher dock scoring and interacted with residues D198, R176, R178, Y131, and D200 in the C6-phosphate region in the Cy-FBPase, it was selected out. Finally, the representative nineteen potential hit compounds were bought from Specs Corporation, as list in Table S1 in the Supporting Information.

The Inhibitory Activities *In Vitro* for Screened Dual-Target Inhibitors against Both Cy-FBA-II and Cy-FBPase.

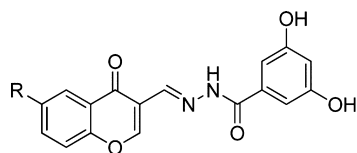
The Cy-FBA-II and Cy-FBPase inhibitor activities of hit compounds screened above are listed in Table S1 in the Supporting Information. As can be seen from Table S1 in the Supporting Information, compounds L1, L12, L18, and L19a exhibited higher inhibitory ratio (>50%) against both Cy-FBA-II and Cy-FBPase, thus, the IC_{50} values of these four compounds were further tested. Fortunately, compound L19a could inhibit not only Cy-FBA-II with IC_{50} of 16.9 μM but also Cy-FBPase with IC_{50} of 100.0 μM , showing more or less dual-target inhibitor’s activities. Thus, compound L19a could be selected as the first generation hit compound for further developing and optimizing to obtain more potent dual-target inhibitors against both Cy-FBA-II and Cy-FBPase.

Optimization of the First/Second Dual-Target Inhibitors. The probable binding models of compound L19a bound into Cy-FBA-II and Cy-FBPase are illustrated in Figures 4A and 4B (magenta sticks), respectively. At the catalytic region in the active site of Cy-FBA-II, our docking results showed that one hydroxyl group on the benzene ring of compound L19a

actually formed one coordination bond with the metal ion and one hydrogen bond with residue D83. The other hydroxyl group was anchored by its interaction with the backbone amide hydrogen of residue S234. Additionally, one hydrogen bond between amino group and residue T278 could be noticed. The carbonyl group on chromone of compound L19a formed one hydrogen bond with residue R281. In the active site of Cy-FBPase, 3,5-dihydroxyl groups on the benzene ring of L19a might form two remarkable hydrogen bonds with residues D198 and D200, respectively, while the carbonyl group on chromone coordinated with one of the metals. The nitrogen atom on acylhydrazone was involved in a hydrogen bond with residue T102. From these pictures, we can notice that compound L19a is able to interact simultaneously with the crucial residues discussed above in the active site of Cy-FBA-II (Co^{2+} , T278) and Cy-FBPase (T102, D198 and D200). This to some extent explains the reason why compound L19a can exhibit inhibitory activities again both enzymes.

In order to obtain hit compounds with higher inhibitory activities again Cy-FBA-II and Cy-FBPase, the structure optimization of compound L19a was further performed according to the binding models of compound L19a and both enzymes (Cy-FBA-II and Cy-FBPase). On one hand, the magenta sticks in Figure 4A and Figure 4B show that the end of chromone of compound L19a was far from surrounding residues and no remarkable interactions between chromone and surrounding residues could be found. Thus, we propose that it is possible to improve interaction between compound L19a and target enzyme by adding a substituent group to the end of chromone. As listed in Table 1, a series of novel hit

Table 1. The Inhibitory Activities of First-Generation Inhibitors against Cy-FBA-II and Cy-FBPase, Together with Corresponding Inhibition against *Synechocystis* sp. PCC 6803



compd	R	IC ₅₀ (μM)		
		Cy-FBA-II	Cy-FBPase	EC ₅₀ ^a (ppm)
L19a	H	16.9 ± 1.4	100.0 ± 15.3	22.3 ± 2.2
L19b	Cl	11.5 ± 0.3	125.7 ± 68.1	8.3 ± 0.6
L19c	Br	4.2 ± 0.7	110.8 ± 56.9	9.3 ± 0.5
L19d	F	14.6 ± 1.1	141.2 ± 12.2	5.0 ± 1.4
L19e	CH ₃	61.7 ± 5.7	103.2 ± 17.3	11.6 ± 7.0
L19f	CH ₂ CH ₃	40.3 ± 4.7	93.9 ± 7.7	9.2 ± 2.5
L19g	CH(CH ₃) ₂	28.1 ± 7.3	77.7 ± 9.6	2.9 ± 0.6
L19h	C(CH ₃) ₃	15.0 ± 2.1	31.5 ± 8.7	6.1 ± 0.5
L19i	NO ₂	2.0 ± 0.2	>200	76.7 ± 9.8

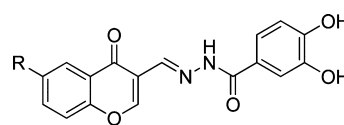
^aThe inhibitory activities against *Synechocystis* sp. PCC 6803.

compounds with similar molecular backbone but different R substituents (L19b–L19i) were synthesized, which were regarded as first-generation dual-target inhibitors.

On the other hand, as discussed above, the metal was critical for the catalysis of Cy-FBA-II; this means that increasing the compound's interactions with metal in Cy-FBA-II would likely give rise to the corresponding compound's Cy-FBA-II inhibitory activities in vitro. Thus, we imagined simply changing

3,5-dihydroxyl groups (L19a–L19i) to 3,4-dihydroxyl groups. The compounds with 3,4-dihydroxyl groups were regarded as second-generation inhibitors (L20a–L20i). This change not only brings about strong bidentate coordination with metal ions in Cy-FBA-II (Figure 4A, yellow sticks) but also keeps the interactions of inhibitors and critical residues (D200 and D198) in the active site of Cy-FBPase (Figure 4B, yellow sticks). The idea was also originated from Mariano and his co-workers' work on the design of *Giardia* FBA inhibitors,⁵ in which the inhibitor with alpha-hydroxy ketone has higher inhibitory activities. Based on this designing strategy, the second-generation hit compounds L20a–L20i were further synthesized (as illustrated in Table 2), together with the corresponding inhibitory activities in vitro and in vivo.

Table 2. The Inhibitory Activities of Second-Generation Inhibitors against Cy-FBA-II and Cy-FBPase, Together with Corresponding Inhibition against *Synechocystis* sp. PCC 6803



compd	R	IC ₅₀ (μM)		
		Cy-FBA-II	Cy-FBPase	EC ₅₀ ^a (ppm)
L20a	H	4.4 ± 0.5	140.1 ± 23.1	15.3 ± 7.0
L20b	Cl	4.4 ± 0.5	107.6 ± 18.9	2.0 ± 2.1
L20c	Br	2.3 ± 0.4	92.0 ± 3.9	0.8 ± 0.1
L20d	F	5.7 ± 0.5	120.5 ± 29.4	10.5 ± 2.7
L20e	CH ₃	14.4 ± 1.3	23.4 ± 2.4	5.3 ± 0.9
L20f	CH ₂ CH ₃	10.6 ± 0.9	19.2 ± 2.5	6.5 ± 1.0
L20g	CH(CH ₃) ₂	22.0 ± 2.8	14.7 ± 2.0	1.6 ± 0.2
L20h	C(CH ₃) ₃	26.7 ± 2.7	14.1 ± 1.9	7.4 ± 1.2
L20i	NO ₂	0.9 ± 0.1	>200	20.7 ± 3.1

^aThe inhibitory activities against *Synechocystis* sp. PCC 6803.

Synthesis of Benzohydrazide Derivatives. As shown in Figure 2, compounds L19a–L19i and L20a–L20i were synthesized by using substituted phenols as starting materials. Substituted phenols 1 were reacted with acetic anhydride in the presence of several drops of concentrated H₂SO₄, respectively, to afford corresponding esters 2. This method is more convenient than previous methods.^{40–44} Subsequently, *o*-hydroxyacetophenone 3 was generated by Fries rearrangement reaction⁴⁵ in moderate yields (about 35%) under the condition of dry powdered AlCl₃. The Vilsmeier–Haack cyclizations^{28,46–48} of *o*-hydroxyacetophenones 3 were reacted with anhydrous DMF and POCl₃ to form substituted 3-formylchromones 4 in a high yield. Additionally, the nitro-substituted compound 4i was prepared by the nitration of 4a. The title compounds L19a–L19i, and L20a–L20i were synthesized by the condensation of compounds 4 and 3,5-(and 3,4)-dihydroxybenzohydrazide in the presence of acetic acid at room temperature, which was similar to previous methods.⁴⁹

SAR Analysis of First/Second Generation of Dual-Target Inhibitors. The Cy-FBA-II and Cy-FBPase inhibitory activities (IC₅₀) of synthesized first-generation dual-target inhibitors with different R group were reported in Table 1, respectively, together with the inhibition in vivo against *Synechocystis* sp. PCC 6803. The inhibitory activity of probe molecule L19a is summarized in Table 1 as well. As can be seen

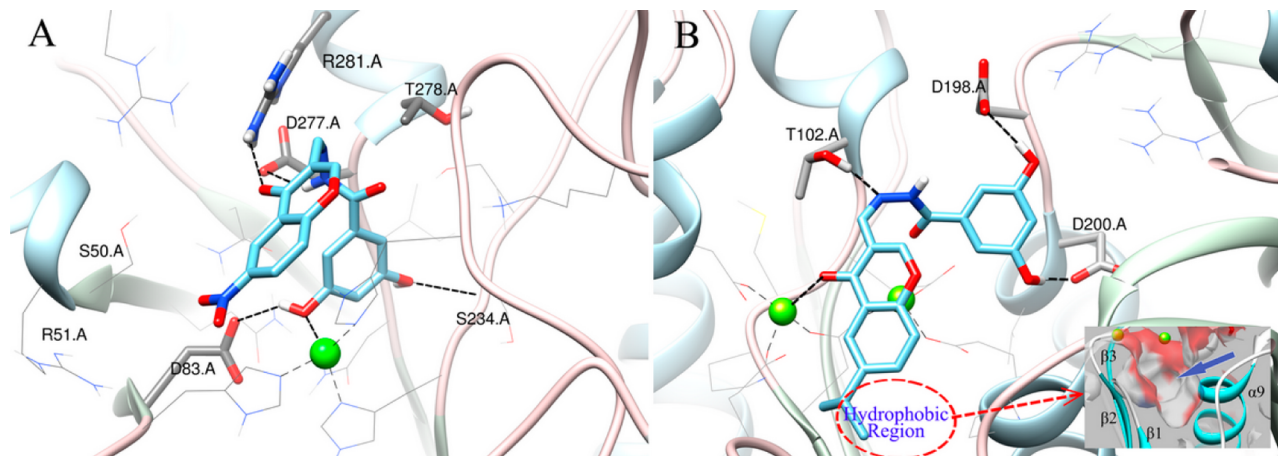


Figure 5. The binding modes of inhibitor **L19i** bound into the active site of Cy-FBA-II (A) and **L19g** bound into the active site of Cy-FBPase (B). The dashed lines indicate the important hydrogen bonds between inhibitor and target enzyme. Inset: surface of the small hydrophobic cavity between three β -strands ($\beta_1-\beta_3$) and one α -helix (α_9), which is labeled by a blue arrow in the vicinity of the hydrophilic pocket.

from Table 1, the effects of R substituents on the Cy-FBA-II and Cy-FBPase inhibitory activities were obvious and different. When the R group was replaced by halogen groups ($-F$, $-Cl$, and $-Br$) and $-NO_2$ group, the compounds (**L19b–L19d** and **L19i**) showed higher Cy-FBA-II inhibitory activities ($IC_{50} = 2.0\text{--}11.5 \mu M$) than probe molecule **L19a** ($IC_{50} = 16.9 \mu M$). Especially, $-Br$ and $-NO_2$ groups at the R position are favorable for Cy-FBA-II inhibitions, which led to a remarkable decrease (about 4-fold) of the Cy-FBA-II IC_{50} value as compared with probe molecule **L19a**. In contrast, compounds **L19b–L19f** exhibited similar Cy-FBPase inhibitory activities compared with probe molecule **L19a**, which indicates that the influences of halogen groups and little hydrophobicity on Cy-FBPase inhibition were indeed subtle. Nevertheless, the larger hydrophobic groups actually were favorable for Cy-FBPase inhibition. For instance, compounds **L19g** and **L19h** exhibit higher Cy-FBPase inhibitory activities ($IC_{50} = 77.7\text{--}31.5 \mu M$) than those of probe molecule **L19a** ($IC_{50} = 100.0 \mu M$). It should be noticed that almost weak Cy-FBPase inhibition ($IC_{50} > 200 \mu M$) was observed for compound **L19i**, thus we have to believe that the NO_2 group is unfavorable for Cy-FBPase inhibition. To explain the reason why R groups have different effects on Cy-FBA-II and Cy-FBPase, compounds **L19i** and **L19g** were taken as example and the binding models of **L19i** target into Cy-FBA-II and **L19g** target into Cy-FBPase are illustrated in Figure 5A and Figure 5B, respectively. As illustrated in Figure 5A, the R group of **L19i** seems positioned into a hydrophilic region constituted by residues: S50, R51, D83, N24, etc.; this docking result suggested that halogen group and hydrophilic groups in R position were favorable in this region. In line with the docking result, compounds **L19b–L19d** and **L19i** actually exhibit higher Cy-FBA-II inhibitory activities than compounds **L19e–L19g**. In comparison, in the pocket of Cy-FBPase, R groups were positioned in a hydrophobic region, thus bulky hydrophobic groups in the R position, such as compounds **L19g** and **L19h**, were favorable for the Cy-FBPase, as illustrated in Figure 5B.

To obtain more potential dual-target inhibitors against Cy-FBA-II and Cy-FBPase, the second-generation dual-target inhibitors (**L20a–L20i**) were further designed, synthesized, and evaluated, as listed in Table 2. When the 3,5-dihydroxy groups of inhibitors (**L19a–L19i**) were changed to 3,4-dihydroxy groups (**L20a–L20i**), the Cy-FBA-II inhibitory

activities of second-generation inhibitors increased more than 2-fold as compared with the first-generation inhibitors (Table 1) except for compounds **L20g** and **L20h**, which in turn result in better EC_{50} values of second-generation inhibitors. For instance, the Cy-FBA-II inhibitory activity of compounds **L20a**, **L20e**, and **L20f** were about 4-fold higher than those of the corresponding compounds **L19a**, **L19e**, and **L19f**, respectively, while the IC_{50} (Cy-FBA-II) of compounds **L20b**, **L20c**, **L20d**, and **L20i** were about 2 times lower than those of the corresponding compounds **L19b**, **L19c**, **L19d**, and **L19i**, respectively. However, compared with first-generation inhibitors, the Cy-FBPase inhibitory activities of second-generation inhibitors exhibit slight change except for **L20e–L20g**. These experimental results confirmed our previous propositions. As shown in Figure 4A, compared with compound **L19a**, two hydroxyls in the benzene ring of compound **L20a** could coordinate with the Co^{2+} in the active site of Cy-FBA-II, which led to the stronger interactions of compound **L20a** and Cy-FBA-II, in turn resulting in the lower IC_{50} (Cy-FBA-II activities) of compound **L20a**. However, in the active site of Cy-FBPase, compound **L20a** kept the interactions between inhibitors and critical residues (D200 and D198), thus the Cy-FBPase inhibitory activities of compound **L20a** were subtly changed compared to compound **L19a**.

For second-generation inhibitors, 3,4-dihydroxy groups have remarkably increased the Cy-FBA-II inhibitions, but the effects of the R group on Cy-FBA-II activities were slight. For instance, compounds **L20b–L20d** and **L20i** show similar Cy-FBA-II inhibitions compared with compound **L20a**, and compounds **L20e–L20h** exhibit similar Cy-FBA-II inhibitions for each other but lower than compound **L20a**. Although 3,4-dihydroxy groups could not affect Cy-FBPase inhibitions, the IC_{50} values of compounds **L20e** ($14.4 \mu M$), **L20f** ($10.6 \mu M$) and **L20g** ($22.0 \mu M$) against Cy-FBPase show striking decrease compared with compounds **L19e**, **L19f**, and **L19g**. This case is likely due to the superposition of effects of 3,4-dihydroxy groups and hydrophobic groups.

In conclusion, with a systematic structure-centric approach, a specific protocol of molecular docking-based dual-target virtual screening was generated and performed for both target enzymes. A series of potential hit compounds interacting with both enzymes were virtually filtered out from the Specs database, and their inhibitory activities were examined *in vitro*

and *in vivo*. Followed by a further study of combining structure–activity relationship (SAR) analysis and optimized synthesis, the first set of novel dual-target inhibitors targeting on both Cy-FBA-II and Cy-FBPase were identified. The experimental results showed that compounds **L19e–L19g** exhibited moderate inhibitory activities ($IC_{50} = 28.1\text{--}103.2 \mu\text{M}$) against both Cy-FBA-II and Cy-FBPase, and compounds **L19a–L19d**, **L19h**, and **L20a–L20d** exhibited high Cy-FBA-II inhibitory activities ($IC_{50} = 2.3\text{--}16.9 \mu\text{M}$) and moderate Cy-FBPase inhibitory activities ($IC_{50} = 31.5\text{--}141.2 \mu\text{M}$); however, compounds **L20e–L20h** could potently inhibit both Cy-FBA-II and Cy-FBPase with IC_{50} values less than 30 μM , which demonstrated more or less dual-target inhibitor's feature. Moreover, most of them exhibited high algicide activity ($EC_{50} = 0.8\text{--}15.3 \text{ ppm}$) against cyanobacteria *Synechocystis* sp. PCC 6803. However, it is hard to make direct correlations between *in vitro* and *in vivo* inhibition tests from the currently available experimental data, because the absorption, distribution, and metabolism performance of individual compounds obtained in the present study are quite different. The positive results indicated all modeling strategies and virtual screening processes presented in the current study most likely to be an encouraging way in the search of new lead compounds with brand-new molecular backbone for the dual-target inhibitors, which may open a new promising route toward developing environmentally acceptable chemical control for the treatment of HABs in the future.

ASSOCIATED CONTENT

Supporting Information

Additional figures and a table as discussed in the text. This material is available free of charge via the Internet at <http://pubs.acs.org>.

AUTHOR INFORMATION

Corresponding Author

*Phone: +86-27-67862022. Fax: +86-27-67862022. E-mail: renyl@mail.ccnu.edu.cn; jianwan@mail.ccnu.edu.cn.

Author Contributions

[§]These authors contributed equally to this study

Funding

This work was supported by the National Basic Research Program of China (973 Program, No. 2010CB126100), the Natural Science Foundation of China (No. 21202056, 21272089, 21172089, 21072073, 20873049), PCSIRT (No. IRT0953), Natural Science Foundation of Hubei Province (No. 2010CDB01202), the Program for Academic leader in Wuhan Municipality (No. 201150530150), and the self-determined research funds of CCNU from the colleges' basic research and operation of MOE (No. CCNU10C01002 and CCNU10A02006).

Notes

The authors declare no competing financial interest.

REFERENCES

- Carmichael, W. W. Health Effects of Toxin-Producing Cyanobacteria: "The CyanoHABs. *Hum. Ecol. Risk Assess.* **2001**, *7*, 1393–1407.
- St-Jean, M.; Blonski, C.; Sygusch, J. Charge Stabilization and Entropy Reduction of Central Lysine Residues in Fructose-Bisphosphate Aldolase. *Biochemistry* **2009**, *48*, 4528–4537.
- Choi, K. H.; Shi, J.; Hopkins, C. E.; Tolan, D. R.; Allen, K. N. Snapshots of Catalysis: The Structure of Fructose-1,6-(bis)phosphate Aldolase Covalently Bound to the Substrate Dihydroxyacetone Phosphate. *Biochemistry* **2001**, *40*, 13868–13875.
- Daher, R.; Coincqn, M.; Fonvielle, M.; Gest, P. M.; Guerin, M. E.; Jackson, M.; Sygusch, J.; Therisod, M. Rational Design, Synthesis, and Evaluation of New Selective Inhibitors of Microbial Class II (Zinc Dependent) Fructose Bis-phosphate Aldolases. *J. Med. Chem.* **2010**, *53*, 7836–7842.
- Li, Z.; Liu, Z.; Cho, D. W.; Zou, J.; Gong, M.; Breece, R. M.; Galkin, A.; Li, L.; Zhao, H.; Maestas, G. D.; Tierney, D. L.; Herzberg, O.; Dunaway-Mariano, D.; Mariano, P. S. Rational design, synthesis and evaluation of first generation inhibitors of the Giardia lamblia fructose-1,6-biphosphate aldolase. *J. Inorg. Biochem.* **2011**, *105*, 509–517.
- Tamoi, M.; Takeda, T.; Shigeoka, S. Functional Analysis of Fructose-1,6-Bisphosphatase Isozymes (fbp-I and fbp-II Gene Products) in Cyanobacteria. *Plant Cell Physiol.* **1999**, *40*, 257–261.
- Iastrebova, O. V. Functioning of fructose-1,6-bisphosphatase—main enzyme of gluconeogenesis in microorganisms. *Ukr. Biokhim. Zh.* **2002**, *74*, 24–32.
- Kaneko, T.; Sato, S.; Kotani, H.; Tanaka, A.; Asamizu, E.; Nakamura, Y.; Miyajima, N.; Hiroseawa, M.; Sugiura, M.; Sasamoto, S.; Kimura, T.; Hosouchi, T.; Matsuno, A.; Muraki, A.; Nakazaki, N.; Naruo, K.; Okumura, S.; Shimpo, S.; Takeuchi, C.; Wada, T.; Watanabe, A.; Yamada, M.; Yasuda, M.; Tabata, S. Sequence analysis of the genome of the unicellular cyanobacterium *Synechocystis* sp. strain PCC6803. II. Sequence determination of the entire genome and assignment of potential protein-coding regions. *DNA Res.* **1996**, *3*, 109–136.
- Nakahara, K.; Yamamoto, H.; Miyake, C.; Yokota, A. Purification and Characterization of Class-I and Class-II Fructose-1,6-bisphosphate Aldolases from the Cyanobacterium *Synechocystis* sp. PCC 6803. *Plant Cell Physiol.* **2003**, *44*, 326–333.
- Tamoi, M.; Murakami, A.; Takeda, T.; Shigeoka, S. Acquisition of a new type of fructose-1,6-bisphosphatase with resistance to hydrogen peroxide in cyanobacteria: molecular characterization of the enzyme from *Synechocystis* PCC 6803. *Biochim. Biophys. Acta* **1998**, *1383*, 232–244.
- Miyagawa, Y.; Tamoi, M.; Shigeoka, S. Overexpression of a cyanobacterial fructose-1,6-/sedoheptulose-1,7-bisphosphatase in tobacco enhances photosynthesis and growth. *Nat. Biotechnol.* **2001**, *19*, 965–969.
- Wermuth, C. G. Multitargeted drugs: the end of the 'one-target-one-disease' philosophy? *Drug Discovery Today* **2004**, *9*, 826–827.
- Moser, D.; Wisniewska, J. M.; Hahn, S.; Achenbach, J.; Buscató, E. I.; Klingler, F.-M.; Hofmann, B.; Steinhilber, D.; Proschak, E. Dual-Target Virtual Screening by Pharmacophore Elucidation and Molecular Shape Filtering. *ACS Med. Chem. Lett.* **2012**, *3*, 155–158.
- Larkin, M. A.; Blackshields, G.; Brown, N. P.; Chenna, R.; McGettigan, P. A.; McWilliam, H.; Valentin, F.; Wallace, I. M.; Wilm, A.; Lopez, R.; Thompson, J. D.; Gibson, T. J.; Higgins, D. G.; Clustal, W. and Clustal X version 2.0. *Bioinformatics* **2007**, *23*, 2947–2948.
- Arnold, K.; Bordoli, L.; Kopp, J.; Schwede, T. The SWISS-MODEL workspace: a web-based environment for protein structure homology modeling. *Bioinformatics* **2006**, *22*, 195–201.
- Bordoli, L.; Kiefer, F.; Arnold, K.; Benkert, P.; Battey, J.; Schwede, T. Protein structure homology modeling using SWISS-MODEL workspace. *Nat. Protoc.* **2008**, *4*, 1–13.
- Cornell, W. D.; Cieplak, P.; Bayly, C. I.; Gould, I. R.; Merz, K. M.; Ferguson, D. M.; Spellmeyer, D. C.; Fox, T.; Caldwell, J. W.; Kollman, P. A. A Second Generation Force Field for the Simulation of Proteins, Nucleic Acids, and Organic Molecules. *J. Am. Chem. Soc.* **1995**, *117*, 5179–5197.
- Wang, D.; Zhu, X.; Cui, C.; Dong, M.; Jiang, H.; Li, Z.; Liu, Z.; Zhu, W.; Wang, J. G. Discovery of Novel Acetohydroxyacid Synthase Inhibitors as Active Agents against Mycobacterium tuberculosis by Virtual Screening and Bioassay. *J. Chem. Inf. Model.* **2013**, *53*, 343–353.

- (19) Laskowski, R. A.; MacArthur, M. W.; Moss, D. S.; Thornton, J. M. PROCHECK: a program to check the stereochemical quality of protein structures. *J. Appl. Crystallogr.* **1993**, *26*, 283–291.
- (20) Wiederstein, M.; Sippl, M. J. ProSA-web: interactive web service for the recognition of errors in three-dimensional structures of proteins. *Nucleic Acids Res.* **2007**, *35*, w407–w410.
- (21) Cristobal, S.; Zemla, A.; Fischer, D.; Rychlewski, L.; Elofsson, A. A study of quality measures for protein threading models. *BMC Bioinf.* **2001**, *2*, 5.
- (22) Benkert, P.; Schwede, T.; Tosatto, S. QMEANclust: estimation of protein model quality by combining a composite scoring function with structural density information. *BMC Struct. Biol.* **2009**, *9*, 35.
- (23) Rarey, M.; Kramer, B.; Lengauer, T.; Klebe, G. A fast flexible docking method using an incremental construction algorithm. *J. Mol. Biol.* **1996**, *261*, 470–489.
- (24) Hindle, S.; Rarey, M.; Buning, C.; Lengauer, T. Flexible docking under pharmacophore type constraints. *J. Comput.-Aided Mol. Des.* **2002**, *16*, 129–149.
- (25) Jain, A. N. Surflex: Fully Automatic Flexible Molecular Docking Using a Molecular Similarity-Based Search Engine. *J. Med. Chem.* **2003**, *46*, 499–511.
- (26) Li, D.; Gui, J.; Li, Y.; Feng, L.; Han, X.; Sun, Y.; Sun, T.; Chen, Z.; Cao, Y.; Zhang, Y.; Zhou, L.; Hu, X.; Ren, Y.; Wan, J. Structure-Based Design and Screen of Novel Inhibitors for Class II 3-Hydroxy-3-methylglutaryl Coenzyme A Reductase from Streptococcus Pneumoniae. *J. Chem. Inf. Model.* **2012**, *52*, 1833–1841.
- (27) Zhang, Q. Y.; Li, D.; Wei, P.; Zhang, J.; Wan, J.; Ren, Y. L.; Chen, Z. G.; Liu, D. L.; Yu, Z. N.; Feng, L. L. Structure-Based Rational Screening of Novel Hit Compounds with Structural Diversity for Cytochrome P450 Sterol 14 alpha-Demethylase from Penicillium digitatum. *J. Chem. Inf. Model.* **2010**, *50*, 317–325.
- (28) Nohara, A.; Umetani, T.; Sanno, Y. Studies on antianaphylactic agents—I: A facile synthesis of 4-oxo-4H-1-benzopyran-3-carboxaldehydes by Vilsmeier reagents. *Tetrahedron* **1974**, *30*, 3553–3561.
- (29) Sun, Y.; Liao, X.; Li, D.; Feng, L.; Li, J.; Wang, X.; Jin, J.; Yi, F.; Zhou, L.; Wan, J. Study on the interaction between cyanobacteria FBP/SBPase and metal ions. *Spectrochim. Acta A* **2012**, *89*, 337–344.
- (30) Seuter, A.; Busch, M.; Hain, R. Overexpression of the potential herbicide target sedoheptulose-1,7-bisphosphatase from Spinacia oleracea in transgenic tobacco. *Mol. Breeding* **2002**, *9*, 53–61.
- (31) Wright, S. W.; Carlo, A. A.; Carty, M. D.; Danley, D. E.; Hageman, D. L.; Karam, G. A.; Levy, C. B.; Mansour, M. N.; Mathiowitz, A. M.; McClure, L. D.; Nestor, N. B.; McPherson, R. K.; Pandit, J.; Pustilnik, L. R.; Schulte, G. K.; Soeller, W. C.; Treadway, J. L.; Wang, I. K.; Bauer, P. H. Anilinoquinazoline inhibitors of fructose 1,6-bisphosphatase bind at a novel allosteric site: synthesis, in vitro characterization, and X-ray crystallography. *J. Med. Chem.* **2002**, *45*, 3865–3877.
- (32) Rudnitskaya, A.; Huynh, K.; Torok, B.; Stieglitz, K. Novel heteroaromatic organofluorine inhibitors of fructose-1,6-bisphosphatase. *J. Med. Chem.* **2009**, *52*, 878–882.
- (33) Hines, J. K.; Kruesel, C. E.; Fromm, H. J.; Honzatko, R. B. Structure of Inhibited Fructose-1,6-bisphosphatase from Escherichia coli: distinct allosteric inhibition sites for amp and glucose 6-phosphate and the characterization of a gluconeogenic switch. *J. Biol. Chem.* **2007**, *282*, 24697–24706.
- (34) Stanier, R. Y.; Kunisawa, R.; Mandel, M.; Cohen-Bazire, G. Purification and properties of unicellular blue-green algae (order Chroococcales). *Bacteriol. Rev* **1971**, *35*, 171–205.
- (35) Martí-Renom, M. A.; Stuart, A. C.; Fiser, A.; Sanchez, R.; Melo, F.; Sali, A. Comparative protein structure modeling of genes and genomes. *Annu. Rev. Biophys. Biomol. Struct.* **2000**, *29*, 291–325.
- (36) Clark, M.; Cramer, R. D.; Van Opdenbosch, N. Validation of the general purpose tripos 5.2 force field. *J. Comput. Chem.* **1989**, *10*, 982–1012.
- (37) Lipinski, C. A.; Lombardo, F.; Dominy, B. W.; Feeney, P. J. Experimental and computational approaches to estimate solubility and permeability in drug discovery and development settings. *Adv. Drug Delivery Rev.* **2012**, *64* (Suppl.), 4–17.
- (38) Polgár, T.; Baki, A.; Szendrei, G. I.; Keserű, G. M. Comparative Virtual and Experimental High-Throughput Screening for Glycogen Synthase Kinase-3 β Inhibitors. *J. Med. Chem.* **2005**, *48*, 7946–7959.
- (39) Jain, A. Surfex-Dock 2.1: Robust performance from ligand energetic modeling, ring flexibility, and knowledge-based search. *J. Comput.-Aided Mol. Des.* **2007**, *21*, 281–306.
- (40) Raju, B. C.; Rao, R. N.; Suman, P.; Yogeeshwari, P.; Sriram, D.; Shaik, T. B.; Kalivendi, S. V. Synthesis, structure–activity relationship of novel substituted 4H-chromen-1,2,3,4-tetrahydropyrimidine-5-carboxylates as potential anti-mycobacterial and anticancer agents. *Bioorg. Med. Chem. Lett.* **2011**, *21*, 2855–2859.
- (41) Cao, L.; Zhang, L.; Cui, P. Synthesis of 3-(3-Alkyl-5-thioxo-1H-4,5-dihydro-1,2,4-triazol-4-yl) aminocarbonylchromones. *Chem. Heterocycl. Compd.* **2004**, *40*, 635–640.
- (42) Paul, S.; Nanda, P.; Gupta, R.; Loupy, A. Ac₂O-Py/basic alumina as a versatile reagent for acetylations in solvent-free conditions under microwave irradiation. *Tetrahedron Lett.* **2002**, *43*, 4261–4265.
- (43) Rao, Y. V. S.; Kulkarni, S. J.; Subrahmanyam, M.; Rao, A. V. R. A novel acylative cyclization reaction of phenol over modified Y zeolites. *Chem. Commun.* **1993**, *0*, 1456–1457.
- (44) Wack, H.; Drury, W. J.; Taggi, A. E.; Ferraris, D.; Lectka, T. Nucleophilic Metal Complexes as Acylation Catalysts: Solvent-Dependent “Switch” Mechanisms Leading to the First Catalyzed Staudinger Reaction. *Org. Lett.* **1999**, *1*, 1985–1988.
- (45) Vrielynck, L.; Cornard, J. P.; Merlin, J. C.; Lautié, M. F. Semi-empirical and vibrational studies of flavone and some deuterated analogues. *Spectrochim. Acta, Part A* **1994**, *50*, 2177–2188.
- (46) Pellegatti, L.; Buchwald, S. L. Continuous-Flow Preparation and Use of β -Chloro Enals Using the Vilsmeier Reagent. *Org. Process Res. Dev.* **2012**, *16*, 1442–1448.
- (47) Wittstein, K.; García, A. B.; Schürmann, M.; Kumar, K. Exploring α -Chromonyl Nitrones as 1,5-Dipoles. *Synlett* **2012**, *2012*, 227–232.
- (48) Borrell, J. I.; Teixidó, J.; Schuler, E.; Michelotti, E. Solid-supported synthetic equivalents of 3-formylchromone and chromone. *Tetrahedron Lett.* **2001**, *42*, 5331–5334.
- (49) Zhou, Z. Z.; Chen, Q.; Yang, G. F. Synthesis and Insecticidal Activities of N-Carbonylamido-2-(4-oxo-4H-1-benzopyran-3-yl)-4-thiazolidinones Derivatives by Microwave-Assisted Parallel Syntheses. *Chin. J. Org. Chem.* **2008**, *28*, 1385–1392.